



Full Length Article

Multidirectional basketball activities load different regions of the tibia: A subject-specific muscle-driven finite element study

Chenxi Yan^a, Ryan J. Bice^b, Jeff W. Frame^b, Stuart J. Warden^{b,c,d,*}, Mariana E. Kersh^{a,e,f,**}

^a Department of Mechanical Science and Engineering, University of Illinois Urbana-Champaign, United States of America

^b Department of Physical Therapy, Indiana University School of Health and Human Sciences, United States of America

^c Indiana Center for Musculoskeletal Health, Indiana University School of Medicine, United States of America

^d La Trobe Sport and Exercise Medicine Research Centre, La Trobe University, Bundoora, Victoria, Australia

^e Beckman Institute for Advanced Science and Technology, University of Illinois Urbana-Champaign, United States of America

^f Carle Illinois College of Medicine, University of Illinois Urbana-Champaign, United States of America



ARTICLE INFO

Keywords:

Bone
Exercise
Physical activity
Running
Stress fracture

ABSTRACT

The tibia is a common site for bone stress injuries, which are believed to develop from microdamage accumulation to repetitive sub-yield strains. There is a need to understand how the tibia is loaded in vivo to understand how bone stress injuries develop and design exercises to build a more robust bone. Here, we use subject-specific, muscle-driven, finite element simulations of 11 basketball players to calculate strain and strain rate distributions at the midshaft and distal tibia during six activities: walking, sprinting, lateral cut, jumping after landing, changing direction from forward-to-backward sprinting, and changing direction while side shuffling. Maximum compressive strains were at least double maximum tensile strains during the stance phase of all activities. Sprinting and lateral cut had the highest compressive ($-2,862 \pm 662 \mu\epsilon$ and $-2,697 \pm 495 \mu\epsilon$, respectively) and tensile ($973 \pm 208 \mu\epsilon$ and $942 \pm 223 \mu\epsilon$, respectively) strains. These activities also had the highest strains rates (peak compressive strain rate = $64,602 \pm 19,068 \mu\epsilon/s$ and $37,961 \pm 14,210 \mu\epsilon/s$, respectively). Compressive strains principally occurred in the posterior tibia for all activities; however, tensile strain location varied. Activities involving a change in direction increased tensile loads in the anterior tibia. These observations may guide preventative and management strategies for tibial bone stress injuries. In terms of prevention, the strain distributions suggest individuals should perform activities involving changes in direction during growth to adapt different parts of the tibia and develop a more fatigue resistant bone. In terms of management, the greater strain and strain rates during sprinting than jumping suggests jumping activities may be commenced earlier than full pace running. The greater anterior tensile strains during changes in direction suggest introduction of these types of activities should be delayed during recovery from an anterior tibial bone stress injury, which have a high-risk of healing complications.

1. Introduction

Bone stress injuries (BSIs), including stress reactions and stress fractures, are a source of frustration in both amateur and professional athletes. They invariably interrupt training due to pain and a real risk of progression to a complete fracture. BSIs are believed to result from mechanical fatigue wherein repetitive loading below yield levels results in the formation of microdamage [1]. Microdamage is a normal phenomenon that triggers targeted remodeling and skeletal renewal. However, an error in workload (e.g., too rapid progression of training)

can promote microdamage accumulation, its coalescence and/or extension, and progression to a BSI [2].

The tibia is one of the most common sites for a BSI, accounting for up to 40% of cases [3–5]. To understand development of BSIs within the tibia, there is a need to understand how the bone is loaded in vivo during activity. Early studies used strain gauges attached to the surface of the tibia to measure bone strain during locomotion [6,7]. In particular, Burr et al. [6] demonstrated that principal strains during vigorous activities (sprinting, zigzag running) were significantly higher than walking. Moreover, sprinting generated the greatest compressive and tensile

* Correspondence to: S.J. Warden, Department of Physical Therapy, Indiana University School of Health and Human Sciences, United States of America.

** Correspondence to: M.E. Kersh, Department of Mechanical Science and Engineering, University of Illinois at Urbana-Champaign, United States of America.

E-mail addresses: stwarden@iu.edu (S.J. Warden), mkersh@illinois.edu (M.E. Kersh).

strain rates. Subsequent studies used strain gauges to explore strains during different activities, and the impact of shoes, neuromuscular fatigue, and running surface, to name a few [8,9]. Most recently, Yang et al. [10] developed an optical segment tracking method involving implantation of bone screws to measure the bending and torsion angle of the tibia during walking and running.

Strain gauge and bone pin implantation methods have advanced our knowledge of tibial loading in vivo but are limited by their invasive nature along with their inability to provide information on the distribution of strains within the volume of bone tissue. Further, previous invasive studies were performed in non-athletes who may have different movement patterns and forces than a trained athletic population.

Computational approaches offer a novel non-invasive method for estimating in vivo tibial bone strains. They involve estimates of musculoskeletal loads applied to the skeleton based on experimental measures of human movement and external forces such as the ground reaction force. Previous studies have used computational approaches to estimate tibial loading during walking and running [11–21]. Ankle and knee joint reaction forces, muscle forces, and ground reaction forces during walking and running at different speeds and slopes were evaluated by inverse dynamics using a rigid body model [11–13]. The joint reaction forces quantified were due to the combined effects of muscle and ground reaction forces, but these loads do not necessarily reflect the strain experienced by the tibia. Analytical models of bone with boundary conditions based on motion analysis have been used to quantify stresses in the tibia during running [14,15]. However, the contribution of tibial geometry and heterogeneous material properties has infrequently been considered. Finite element (FE) models provide the opportunity to analyze bone mechanics under conditions that are difficult to measure in vivo.

The inclusion of muscle forces derived from rigid body musculoskeletal models has now become more widely used as a means for assessing the loading of bone during locomotive tasks, with much attention on the femur [22–24]. Using a similar approach, tibial loading and deformation during walking have been analyzed [16–18,20], with model predictions of tibial deformation and strain being consistent with previous in vivo experiments [6,7]. However, less is known about the distribution of strains within the tibia during vigorous, multidirectional tasks. Characterizing the physiological strain environment of bone can provide insight into areas potentially at risk of injury as well as areas that may undergo site-specific adaptation.

The aim of the current study was to estimate tibial bone strain magnitudes and rates during vigorous activities using subject-specific musculoskeletal modeling and a CT-based FE model of the tibia. Activities involving sudden changes in direction were included to explore the distribution of strains in bone volumes at both the midshaft tibia (mid-tibia) and junction of the proximal 2/3 and distal 1/3 of the tibia (distal tibia). The study was performed in collegiate-level basketball players as they are trained to perform activities with sudden changes in direction and are at risk of tibial bone stress injuries [25].

2. Methods

2.1. Participants

Male basketball players competing at the Division I, II or III level within the National Collegiate Athletic Association were recruited via convenience sampling from local universities and colleges. Participants were ineligible if they reported a history of: 1) tibia or fibula stress fracture or fracture; 2) lower extremity injury in the past 6 months that precluded participation in any basketball activities, or; 3) lower extremity surgery or immobilization for longer than 2 weeks in the past 2 years. The study was approved by the Institutional Review Board of Indiana University and all participants provided written informed consent.

2.2. Testing protocol

Testing was performed in a biomechanics laboratory equipped with a 10-camera motion capture system (VICON Vero v2.2, Oxford, UK) synchronized with an in-ground force platform (AMTI OR6-7, Watertown, MA). Participants were provided a standardized basketball shoe (Nike Air Behold Low Basketball Shoe, Nike Inc., Beaverton, OR), chosen for its low cut and smooth synthetic upper to promote foot marker adherence. Retro-reflective markers were positioned on 28 upper and lower body landmarks, based on an established marker set [26]. Locations were initially demarcated with a semi-permanent pen before the retro-reflective markers were affixed using double sided tape and secured using Coban wrap (3M Company, St. Paul, MN), Cover-Roll stretch tape (BSN Medical Inc., Charlotte, NC), and/or Transpore surgical tape (3M Company, St. Paul, MN).

Following a 5-minute warm-up of treadmill running at a self-selected speed, a static standing calibration trial was performed before subjects completed six different activities (see Table 1 for activity descriptions). During each activity, kinematic and kinetic data were collected at 240 Hz and 2400 Hz, respectively. Each maneuver was repeated until three trials were successfully completed. A successful trial was defined as when the foot of the dominant leg landed completely within the boundaries of the force platform. The dominant leg was the leg opposite the preferred shooting arm, consistent with the concept of crossed symmetry [27].

2.3. Computed tomography

The tibia in the dominant leg was imaged on a multislice CT scanner (Biograph128 mCT; Siemens Healthcare, Knoxville, TN) operating at 120 kVp, 90 mAs, 128×0.6 collimation, and pitch 0.8. The scan region prescribed from a scout scan included the entire tibia from the tibiofemoral to talocrural joint. The scan volume included a calibration phantom containing calcium hydroxyapatite standards embedded in water-equivalent resin (QCT-Bone Mineral Phantom; Image Analysis, Inc., Columbia, KY). Images were axially reconstructed at 1.0 mm slice thickness using a B60s convolution kernel, 512×512 matrix and reconstruction diameter of 35.2 cm (reconstructed voxel size = $0.688 \times 0.688 \times 1.0$ mm³).

2.4. Computational modeling

Loading of the tibia during the stance phase of each task was calculated using muscle-driven FE models based on an established

Table 1
Activities assessed.

Activity	Abbreviation	Description
Walking	Walk	Walking at subjects normal speed (reference activity to which other activities were compared)
Sprinting	Sprint	Running forward in a straight line at maximum speed
Land-jump movement	Jump	Stepping off an 18-inch-high platform, landing on both feet simultaneously, before a maximum vertical jump
Forward-to-backward sprinting	SprintFB	Sprinting forward before planting the dominant leg ^a on the force plate and changing direction to sprint backward
Lateral shuffle	Shuffle	Side stepping at maximum speed to the side of the dominant leg ^a before planting on the force plate and changing direction to sidestep in the opposite direction
Lateral cut	Lateral cut	Sprinting forward in a straight line before planting the dominant leg ^a at the force plate and cutting at an angle of 45° toward the non-dominant leg side

^a The dominant leg was defined as the leg opposite the preferred shooting arm.

computational pipeline [22,28]. For all tasks, kinematic and force plate data were first processed through Matlab (MathWorks, Natick, MA, USA) using the Biomechanical ToolKit package for MATLAB. The kinematic and ground reaction force data were filtered using a lowpass filter with a cutoff frequency of 6 Hz. The stance phase was identified as the time when the force exceeded 1% of the maximum vertical ground reaction force for the trial being analyzed. The end of the stance phase was defined as when the ground reaction force returned to zero. Using OpenSim v3.3 [29,30], anthropometric data of a generic rigid body musculoskeletal model (Gait2354) [31] was linearly scaled to each subject using marker positions acquired during the static trial. Next, joint angles and torques at the knee and ankle joints were calculated using inverse kinematics and inverse dynamics. The resulting forces included the compressive and shear forces acting on both ends of the tibia from those joints. Estimates of muscle forces of the lower limb were calculated using static optimization based on a minimization of muscle activation criteria. The joint reaction force at the knee and ankle were calculated by solving for equilibrium of the tibia. The ankle joint reaction force acting on the tibia was calculated using the joint reaction analysis and exported in the tibial reference system. Muscle and joint forces during the stance phase of each task were time-normalized and discretized into 20 time points.

Subject-specific FE models were created based on the CT images. Within each CT scan, the tibia was manually segmented and converted into triangulated surface meshes using Amira (Thermo Fisher Scientific, Waltham, MA, USA). The surface meshes were then smoothed and exported as solid models (Geomagic, 3D Systems, NC, USA). Each tibia was meshed using quadratic tetrahedral elements (average element number = $541,883 \pm 159,882$; nominal element side length = 1.5 mm, Abaqus, Dassault Systemes, France). The Hounsfield units associated with each element were converted to apparent density using the calibration phantom included in each scan after which a Young's modulus value was assigned to the element based on empirically derived data from the tibia [32]. Assignment of isotropic material properties was

performed using Bonemat with an average of 191 material properties used [33]. The Young's modulus of the cortical bone regions were between 17 and 21 GPa, consistent with previous analyses [34]. The Poisson's ratio was set to 0.3 [34].

Fourteen muscles with insertions at the tibia were modeled using the line of action described within the rigid body musculoskeletal model (Fig. S1). Using common anatomical landmarks, the musculoskeletal model coordinate system was transformed to the FE model coordinate system after which muscle attachment points on the FE model were identified (Fig. 1B, center). The insertion areas for each muscle were approximated using an anatomical atlas [35]. Local anatomical landmarks as well as the relative size of the insertions in the proximal-distal and medial-lateral directions described by Schuenke et al. were used as guides for the manual selection of nodes that represented each insertion area. The total muscle force was evenly distributed along the surface nodes of each insertion area to minimize stress concentrations. All models were visually inspected to ensure consistency in the size and shape of the insertion areas relative to each subjects' individual anatomy [35]. The proximal end of the tibia was fully constrained and five axial springs ($k = 300 \text{ N/mm}$) centered at the distal tibia were used to model passive constraints of the ankle joint [36]. The ankle joint reaction forces were applied to the distal articulating surface of the tibia, and the loads were evenly distributed over the surface nodes. A linear implicit analysis was used to calculate the principal strains in the tibia during the stance phase of each task.

2.5. Data reduction and statistical analyses

All FE models were aligned to a common coordinate system and 10 mm-thick volumes of interest were identified at the mid-tibia and distal tibia (Fig. 1B, right). Analyses of strains and strain rates were based on bone elements only, excluding elements within the bone marrow region (Fig. 1C, left).

For each subject and task, the 95th percentile for tensile and

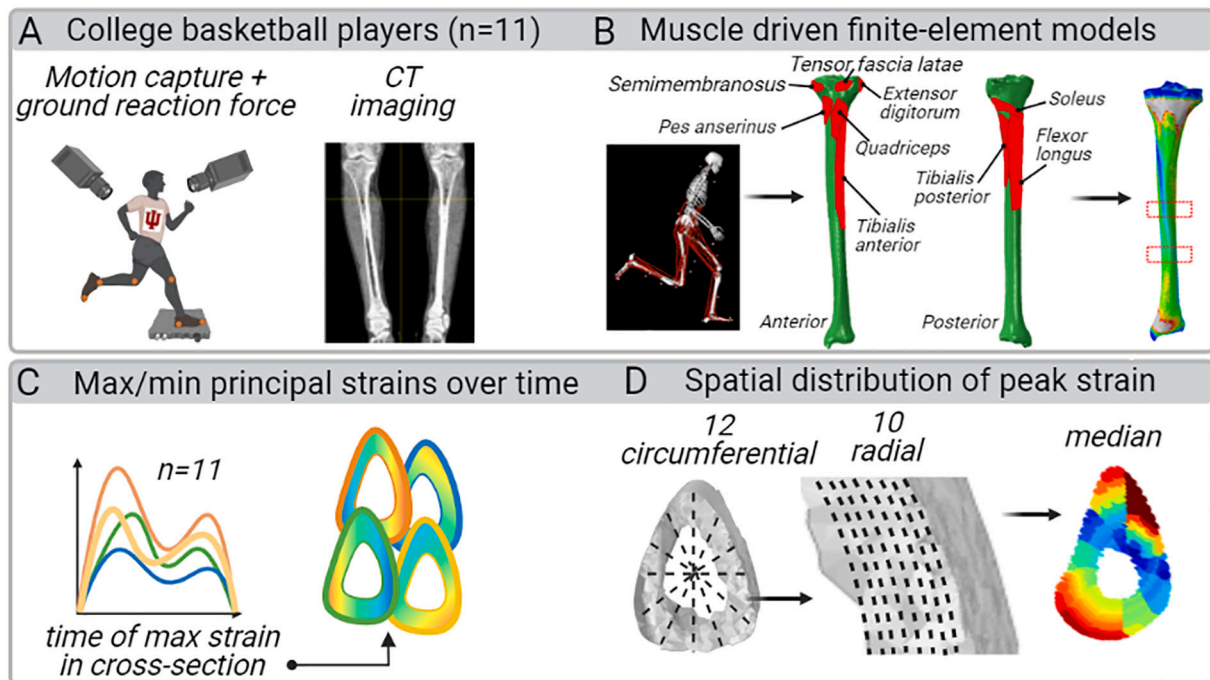


Fig. 1. Diagrammatic representation of the experimental procedures. A) Biomechanics data of college-level basketball players ($n = 11$) performing different activities were collected along with CT images of the lower limbs. B) Data were used to create muscle-driven FE models to investigate loading at the mid-tibia and distal tibia. Nodal surfaces (shown in red) were defined for each muscle insertion area over which muscle forces were distributed. C) For each task, the maximum and minimum principal strains during the stance phase were calculated per subject and D) used to analyze the spatial distribution of the principal strains between activities. (For interpretation of the references to colour in this figure legend, the reader is referred to the web version of this article.)

compressive principal strains within the bone were calculated at each time point during the stance phase (Fig. 1C). The time of peak strain during the stance phase was identified and subsequently used to evaluate the spatial distribution of principal strains. All models were spatially normalized to a common template by calculating the centroid of the cross-section and separating each volume into 12 circumferential zones which were further subdivided into ten radial sections (Fig. 1D, left). The tensile and compressive principal strains, at the time of peak strains, were then compared within the 120 discretized regions (Fig. 1D, right). Strain rate was calculated by numerically differentiating the strain data with respect to time. The same analysis described for maximum and minimum principal strains were repeated for strain rate at both tibial locations.

All post-processing of data was performed in Matlab and Rstudio (RStudio Team (2016); RStudio: Integrated Development for R. RStudio, Inc., Boston, MA) was used for statistical analyses. Peak strain data from each subject and activity were normally distributed, as assessed through Shapiro-Wilks tests. One-way ANOVA tests were used to compare strains and strain rates between activities. Paired *t*-tests were used to compare the strains at identical spatial positions including Bonferroni *p*-value adjustment for multiple comparisons. Post-hoc comparisons of mean strains between different activities were carried out using Tukey HSD tests. Significance was defined as $\alpha = 0.05$.

3. Results

Thirteen participants were recruited. Data from two participants were not included in analyses because of: 1) camera failure negating the ability to complete testing and 2) unrecoverable errors in post-processing of kinematic data. The 11 included participants were 22.7 ± 1.3 years old, 1.93 ± 0.10 m tall, and weighed 91.9 ± 13 kg. During Sprint, subjects ran with an average speed of 6.97 ± 0.27 m/s.

3.1. Mid-tibia compressive strains

During all maneuvers, maximum compressive strains were at least double those of maximum tensile strains at the mid-tibia (Fig. 2A, Table 2). Sprint resulted in the highest compressive strains ($-2,862 \pm 662 \mu\epsilon$), which were 2.5 times greater than Walk ($p = 0.006$) and occurred at 40% of the stance phase (Table 2). Maximum strains during Sprint were spatially located in the posterior region of the tibia (Fig. 2A); however, 88% of the mid-tibia had compressive strains significantly greater than those during Walk (Fig. 2B).

Lateral cut generated the second highest compressive strains ($-2,697 \pm 495 \mu\epsilon$), which were 2 times higher than Walk ($p < 0.001$) and occurred at mid-stance (51% of stance) (Table 2). Like Sprint, the maximum compressive strains during a Lateral cut occurred in the posterior region (Fig. 2A), with 49% of the tibia having strains greater than Walk (Fig. 2B). Sprint and Lateral cut had the shortest stance phases (0.18 ± 0.02 s and 0.27 ± 0.05 s, respectively) (Table 2).

Compressive strains at the mid-tibia were elevated during Jump and Shuffle compared to Walk (all $p < 0.01$) (Table 2). Eighty-four percent and 37% of the mid-tibia had increased strain during Jump and Shuffle compared to Walk, respectively (Fig. 2B). The increased compressive strains during Jump and Shuffle were in the posterior-lateral region (Fig. 2A). There was no difference in mean peak compressive strain between SprintFB and Walk ($p = 0.06$) (Table 2).

3.2. Mid-tibia tensile strains

While lower in magnitude than compressive strains, peak tensile strains during Sprint and Lateral cut were greater than those during Walk (all $p < 0.01$) (Table 2). Peak tensile strain during Sprint ($973 \pm 208 \mu\epsilon$) was 2.6 times higher than during Walk (Table 2) and occurred in the posterior region (Fig. 2A); although tensile strains were elevated in the entire mid-tibia (Fig. 2B). Lateral cut resulted in 2.4-fold greater tensile strains than Walk (Table 2), but unlike Sprint or Walk the region

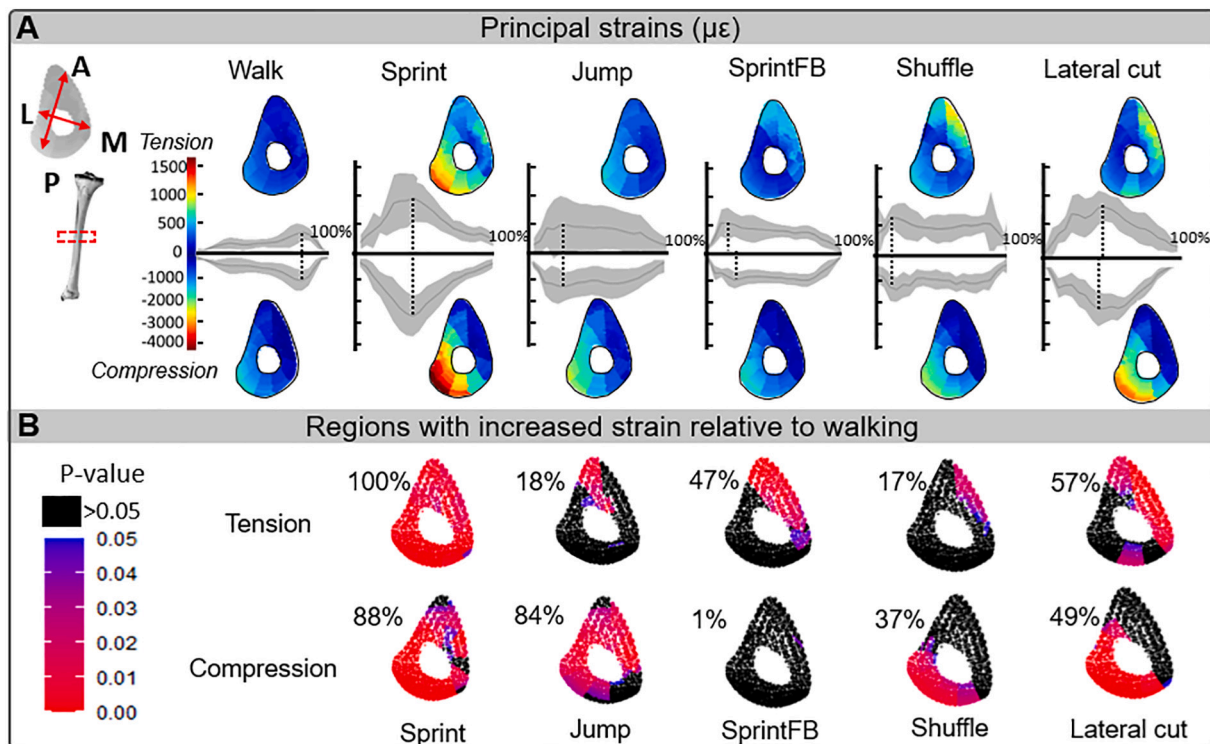


Fig. 2. (A) Maximum tensile (upper images and graphs) and compressive (lower images and graphs) strains at the mid-tibia during the stance phase of each activity. Bounds represent distribution across all subjects and vertical line indicates time of maximum strain. Inset figures of the tibial cross-sections show the distributions of strain at the time of maximum strain during stance. (B) Regions of significantly increased strain relative to Walk.

Table 2

Maximum (tensile) and minimum (compressive) principal strains and strain rates at the mid-tibia during the stance phase of each task and in comparison to Walk.^a

	Walk	Sprint	Jump	SprintFB	Shuffle	Lateral cut
Stance duration (s)	0.72 ± 0.05	0.18 ± 0.02	0.50 ± 0.11	0.64 ± 0.19	0.59 ± 0.14	0.27 ± 0.05
Peak strain (µε)						
Compressive	-1,131 ± 490	-2,862 ± 662 ^c	-1,730 ± 617 ^c	-1,347 ± 317	-1,718 ± 655 ^c	-2,697 ± 495 ^c
Compared to Walk		(p = 0.004)	(p < 0.001)	(p = 0.6)	(p = 0.003)	(p < 0.001)
Fold diff. to Walk		2.5	1.5	1.2	1.5	2.4
Time (% of stance) ^b	78 ± 2.3	40 ± 5.1	30 ± 13.8	46 ± 30.7	30 ± 28	51 ± 8.3
Tensile	381 ± 144	973 ± 208 ^c	573 ± 505 ^c	663 ± 217	807 ± 290 ^c	942 ± 223 ^c
Compared to Walk		(p = 0.006)	(p = 0.004)	(p = 0.06)	(p = 0.002)	(p < 0.001)
Fold diff. to Walk		2.6	1.4	1.7	2.1	2.4
Time (% of stance) ^b	79 ± 3	39 ± 4	24 ± 9	25 ± 20	28 ± 28	42 ± 12
Peak strain rate (µε/s)						
Compressive	15,512 ± 9,115	64,602 ± 19,068 ^c	26,518 ± 12,998	19,493 ± 8,594	25,925 ± 13,421	37,961 ± 14,210 ^c
Compared to Walk		(p < 0.001)	(p = 0.15)	(p = 0.55)	(p = 0.37)	(p < 0.001)
Fold diff. to Walk		4.1	1.7	1.2	1.7	2.5
Time (% of stance) ^b	83.5 ± 27.7	15 ± 10.3	18.5 ± 25.5	8.5 ± 7.8	23.9 ± 33.4	20 ± 17.7
Tensile	6,180 ± 3,398	20,640 ± 15,207 ^c	10,556 ± 6,632 ^c	8,107 ± 2,777	9,146 ± 8,856 ^c	18,693 ± 7,402 ^c
Compared to Walk		(p < 0.001)	(p = 0.03)	(p = 0.6)	(p = 0.015)	(p < 0.001)
Fold diff. to Walk		3.3	1.7	1.3	1.5	3.0
Time (% of stance) ^b	92 ± 3	17 ± 10	10 ± 5	9 ± 8	30 ± 40	19 ± 18

^a Data represent mean ± SD.

^b Time of peak strain and strain rate are expressed relatively as a percentage of stance duration for the task.

^c Indicates significant difference compared to Walk.

of increased tensile strains during Lateral cut were in the anterior-medial region of the mid-tibia (Fig. 2A, B). Maximum tensile strains during Jump and Shuffle were also significantly higher than Walk (all p < 0.01) with tensile strains elevated in the anterior region of the tibia (Fig. 2A, B). For SprintFB, 47% of the mid-tibia experienced increased tensile strains compared to Walk with the strains being located in the anteromedial region (Fig. 2A, B). For all activities, the timing of peak tensile strains were similar to those for peak compressive strains (Table 2).

3.3. Mid-tibia compressive strain rates

Similar to strain magnitudes, compressive strain rates at the mid-tibia were greater than tensile strain rates for all activities (Table 2, Fig. 3). However, the timing of maximum strain rate occurred earlier during each task compared to the time of maximum strain. The compressive strain rate at the mid-tibia during Sprint (64,602 ± 19,068 µε/s) was 4.1 times higher than that of Walk (p < 0.001) and occurred near initial contact (15% of stance phase) (Table 2). Compressive strain rates during Lateral cut were 2.45 times higher than that of Walk (p <

0.001) and occurred at 20% of the stance phase (Table 2). During both Sprint and Lateral cut, compressive strain rates were greatest in the posterolateral regions of the mid-tibia (Fig. 3). Compressive strain rates at the mid-tibia during Jump, SprintFB and Shuffle did not differ from Walk (Table 2).

3.4. Mid-tibia tensile strain rates

Tensile strain rates at the mid-tibia during Sprint, Lateral cut, Jump and Shuffle were 3.3, 3.0, 1.7 and 1.5-fold higher than strain rates during Walk, respectively (all p < 0.02) (Table 2). The maximum tensile strain rate occurred in the anteromedial and posterolateral aspects of the mid-tibia during Sprint and in the anteromedial region during Lateral cut and Shuffle (Fig. 3). The timing of maximum tensile strain rates was similar to the timing of maximum compressive strain rate (Table 2).

3.5. Distal tibia strains and strain rates

Overall, similar results were found for the distal tibia with Sprint and

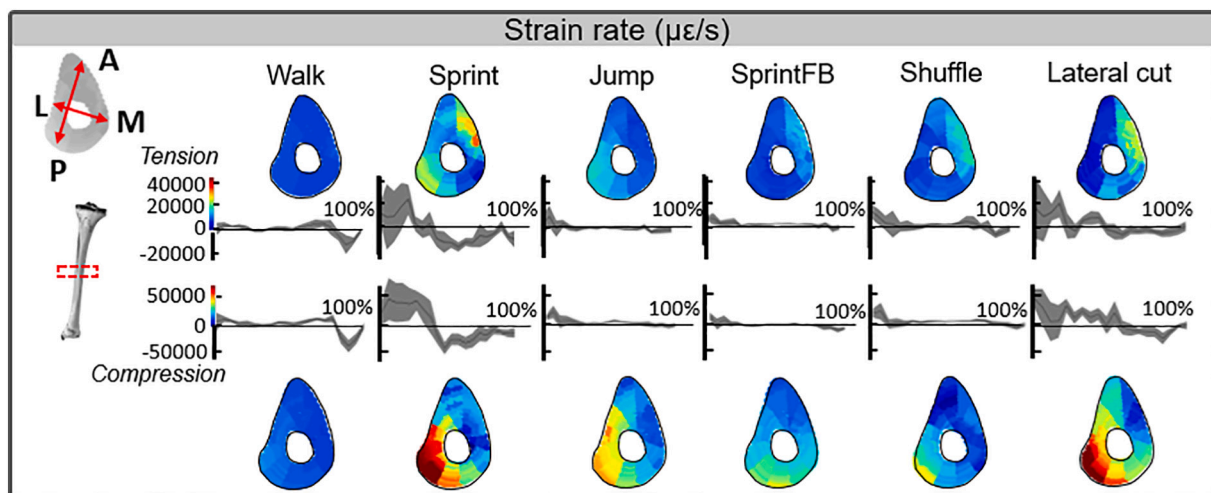


Fig. 3. Maximum tensile (upper images and graphs) and compressive (lower images and graphs) strain rates at the mid-tibia during the stance phase of each activity. Bounds represent distribution across all subjects and vertical line indicates time of maximum strain rate. Inset figures of the tibial cross-sections show the distributions of strain rates at the time of maximum strain rate during stance.

Lateral cut having higher tensile and compressive strains compared to Walk (Table S1, Fig. S2, $p < 0.03$). The distributions of strain within the distal tibia generally mirrored those of the mid-tibia; however, the magnitude of strains was lower at the distal tibia. The timing of maximum strains in the distal tibia was within 3% of the timing of maximum strains at the mid-tibia. As we found for the mid-tibia, tensile and compressive strain rates during Sprint and Lateral cut were higher than Walk (Fig. S3, $p \leq 0.001-0.03$).

4. Discussion

We evaluated the magnitude and distribution of strains and strain rates at the mid-tibia and distal tibia using computational methods. Our results indicate the tibia experienced higher compressive strains than tensile during all activities. Sprint and Lateral cut resulted in the highest strains and strain rates. During these activities, peak strains occurred near midstance, while peak strain rates occurred between initial contact and midstance. Peak compressive strains for all activities tended to be located in the posterior region, while the locations of peak tensile strains were activity-dependent.

Our calculated peak tensile strains during walking ($381 \pm 144 \mu\epsilon$) are striking similar to those reported by Xu et al. [16] ($372 \pm 93 \mu\epsilon$ in tension) who also used FE based simulations. Our maximum compressive strains during walking ($-1,131 \pm 490 \mu\epsilon$) were nearly 1.5 times higher than those reported previously ($-716 \pm 204 \mu\epsilon$), but were consistent with respect to their posterior location and timing during the stance phase of the gait cycle [16–18]. When comparing loading during different activities, studies using strain gauges found compressive strains during running were 2.96 times higher than during walking, and tensile strains were 1.95 times higher [6]. These fold differences are comparable to our data where compressive strains during Sprint were 2.5 times higher than during Walk and tensile strains were 2.6 times higher, despite the higher average running speed of participants in our study (6.97 m/s vs. 2.8–4.7 m/s [6,37]).

Previous studies of strains during a basketball rebounding activity reported average tensile strains of $1592 \mu\epsilon$ and compressive strains of $3163 \mu\epsilon$ [38], which are higher than our calculations during Jump. Differences in methodology (strain gauges vs. computational analyses), subject age (27–52 years old vs 22.7 ± 1.3 years old), and experience level (non-athletes vs. college-level basketball players) may contribute to the observed differences. In terms of experience level, participation in basketball has been shown to enhance tibial bone properties which may in turn decrease the strains generated during basketball maneuvers relative to the same maneuvers performed by non-athletes [39,40]. We have previously shown adaptation-induced reductions in stress and strain during loading in both animal and human studies [27,35]. Also, Wang and colleagues [19] recently reported lower tibial strains in basketball players during walking and load carriage when compared to runners, as determined using computational approaches. Interestingly, the strain rates generated by our subjects during Jump were higher than those measured by Milgrom and colleagues [38]. However, the latter study tested non-athletes whom may perform the task differently than our trained collegiate-level athletes who had a baseline assessed vertical leap of 67.7 ± 6.1 cm.

We found the highest strains and strain rates were concentrated in the posterior region of both the mid- and distal tibia. The posterior location of strains is consistent with previous studies reporting on tibial stress during running [14,15,42]. In particular, Meardon et al. [15] reported higher stresses in the posterior region of the distal tibia during running which were further elevated in runners with a history of tibial bone stress injuries. The higher strains and strain rates in the posterior region of the tibia also fits with clinical data which report 75–90% of tibial bone stress injuries occur in this region [43,44].

Tensile strains and strain rates in the current study were lower in magnitude than compressive strains and strain rates, and their location were dependent on the activity being assessed. Activities involving a

change in direction (i.e. SprintFB, Shuffle, and Lateral cut) resulted in increased tensile strains in the anterior aspect of the tibia. The clinical implications of these observations are two-fold. First, activities involving changes in direction have the potential to increase bone stress injury risk at the anterior tibia, a site at high-risk for healing complications. Although the tensile strains were lower than compressive strains, energy dissipation (which is related to increased microcrack formation) occurs more rapidly under tension than compression during the early stages of fatigue [45]. Introduction of activities involving changes in direction should be delayed during recovery from anterior tibial bone stress injuries, which are at high risk of healing complications. Second, the increased anterior tensile strains indicate that individuals should perform activities involving changes in direction during the permissive period of skeletal growth in order to load more of the tibial cross-section and build a more robust skeletal structure [2,39]. Runners and infantry who played ball sports were at decreased risk of future bone stress injuries [38,46] and loading-induced adaptation in an animal model was shown to exponentially improve bone fatigue resistance [41].

The current study has several strengths, including being the first to utilize a complete subject-specific finite-element model to estimate tibial strains during a range of multi-directional tasks. However, the study also possesses limitations. Our study is limited by a relatively small sample size ($n = 11$); however, the sample size is greater than strain gauge studies which typically involve <5 participants and consistent with computational studies of this type which are labor-intensive. We only assessed principal strains and in two discrete volumes of the tibia, yet the sites assessed are clinically relevant in terms of bone stress injury risk. All activities were performed under strict laboratory conditions where the movements and loads may not fully replicate those occur during actual game play. We studied collegiate-level basketball players because they were highly trained in the activities being assessed. The results might not be fully applicable to other populations. In addition, linear elastic material properties were assumed for bone properties and the tibia-fibula joint reaction force was not included because our analyses were focused at the middle and distal tibia. Future studies investigating more proximal tibial bone loads may benefit from inclusion of the fibula joint reaction force. While we did not perform a convergence analysis, a nominal element length of 1.5 mm has been shown to produce repeatable results when analyzing tibial stiffness [47].

This study used an experimental and modeling approach to analyze the magnitude and distribution of strains and strain rates in the tibia during different activities. We have shown that the tibia is under greater compressive than tensile strains during all tested activities. Maximum compressive strains and strain rates were concentrated in the posterior region where tibial bone stress injuries commonly occur [43,44]. Sprint induced the highest strain and strain rates in the posterior region, which correlates with the location of bone stress injuries in runners. Conversely, the elevated tensile strains in the anterior tibia during movements involving changes in direction may be beneficial for adapting this region of bone when young to prevent anterior tibial bone stress injuries, which have a high risk of healing failure. More longitudinal studies are needed to determine the outcomes of dynamic loading on tibial adaptation and bone stress injury risk to more fully inform the development of training programs.

Supplementary data to this article can be found online at <https://doi.org/10.1016/j.bone.2022.116392>.

CRedit authorship contribution statement

Chenxi Yan: Methodology, Software, Validation, Formal analysis, Investigation, Data curation, Writing – original draft, Visualization. **Ryan J. Bice:** Resources, Data curation. **Jeff W. Frame:** Resources, Data curation. **Stuart J. Warden:** Conceptualization, Methodology, Validation, Investigation, Resources, Data curation, Writing – review & editing, Supervision, Project administration, Funding acquisition. **Mariana**

E. Kersh: Conceptualization, Methodology, Validation, Investigation, Resources, Data curation, Writing – review & editing, Supervision, Project administration, Funding acquisition.

Acknowledgement

This study was supported by the National Basketball Association/General Electric Healthcare Orthopedics and Sports Medicine Collaboration and National Institutes of Health (P30 AR072581). We are grateful for the help of Ida Ang and Woojae Kim with initial data processing.

References

- [1] D.B. Burr, M.R. Forwood, D.P. Fyhrie, R.B. Martin, M.B. Schaffler, C.H. Turner, Bone microdamage and skeletal fragility in osteoporotic and stress fractures, *J. Bone Miner. Res.* 12 (1) (1997 Jan) 6–15, <https://doi.org/10.1359/jbmr.1997.12.1.6>. PMID: 9240720.
- [2] S.J. Warden, W.B. Edwards, R.W. Willy, Preventing bone stress injuries in runners with optimal workload, *Curr Osteoporos Rep.* 19 (3) (2021 Jun) 298–307, <https://doi.org/10.1007/s11914-021-00666-y>. Epub 2021 Feb 26. PMID: 33635519; PMCID: PMC8316280.
- [3] K.L. Bennell, P.D. Brukner, Epidemiology and site specificity of stress fractures, *Clin. Sports Med.* 16 (2) (1997 Apr) 179–196, [https://doi.org/10.1016/s0278-5919\(05\)70016-8](https://doi.org/10.1016/s0278-5919(05)70016-8). PMID: 9238304.
- [4] J. Iwamoto, T. Takeda, Stress fractures in athletes: review of 196 cases, *J. Orthop. Sci.* 8 (3) (2003) 273–278, <https://doi.org/10.1007/s10776-002-0632-5>. PMID: 12768465.
- [5] B.R. Waterman, B. Gun, J.O. Bader, J.D. Orr, P.J. Belmont Jr., Epidemiology of lower extremity stress fractures in the United States military, *Mil. Med.* 181 (10) (2016 Oct) 1308–1313, <https://doi.org/10.7202/MILMED-D-15-00571>. PMID: 27753569.
- [6] D.B. Burr, C. Milgrom, D. Fyhrie, M. Forwood, M. Nyska, A. Finestone, S. Hoshaw, E. Saiaq, A. Simkin, In vivo measurement of human tibial strains during vigorous activity, *Bone* 18 (5) (1996 May) 405–410, [https://doi.org/10.1016/8756-3282\(96\)00028-2](https://doi.org/10.1016/8756-3282(96)00028-2). PMID: 8739897.
- [7] L.E. Lanyon, W.G. Hampson, A.E. Goodship, J.S. Shah, Bone deformation recorded in vivo from strain gauges attached to the human tibial shaft, *Acta Orthop. Scand.* 46 (2) (1975 May) 256–268, <https://doi.org/10.3109/17453677508989216>. PMID: 1146518.
- [8] P.F. Yang, G.P. Brüggemann, J. Rittweger, What do we currently know from in vivo bone strain measurements in humans? *J. Musculoskelet. Neuronal Interact.* 11 (1) (2011 Mar) 8–20. PMID: 21364270.
- [9] R. Al Nazer, J. Lanovaz, C. Kawallak, J.D. Johnston, S. Kontulainen, Direct in vivo strain measurements in human bone—a systematic literature review, *J. Biomech.* 45 (1) (2012 Jan 3) 27–40, <https://doi.org/10.1016/j.jbiomech.2011.08.004>. Epub 2011 Sep 1. Erratum in: *J. Biomech.* 2012 Feb 2;45(3):623. PMID: 21889149.
- [10] P.F. Yang, M. Sanno, B. Ganse, T. Koy, G.P. Brüggemann, L.P. Müller, J. Rittweger, Torsion and antero-posterior bending in the in vivo human tibia loading regimes during walking and running, *PLoS One* 9 (4) (2014 Apr 14), e94525, <https://doi.org/10.1371/journal.pone.0094525>. PMID: 24732724; PMCID: PMC3986088.
- [11] E.S. Matijevich, L.M. Branscombe, L.R. Scott, K.E. Zelik, Ground reaction force metrics are not strongly correlated with tibial bone load when running across speeds and slopes: implications for science, sport and wearable tech, *PLoS One* 14 (1) (2019 Jan 17), e0210000, <https://doi.org/10.1371/journal.pone.0210000>. PMID: 30653510; PMCID: PMC6336327.
- [12] S. Sasimontonkul, B.K. Bay, M.J. Pavol, Bone contact forces on the distal tibia during the stance phase of running, *J. Biomech.* 40 (15) (2007) 3503–3509, <https://doi.org/10.1016/j.jbiomech.2007.05.024>. Epub 2007 Jul 26 PMID: 17662295.
- [13] S.H. Scott, D.A. Winter, Internal forces of chronic running injury sites, *Med. Sci. Sports Exerc.* 22 (3) (1990 Jun) 357–369. PMID: 2381304.
- [14] H. Rice, G. Weir, M.B. Trudeau, S. Meardon, T. Derrick, J. Hamill, Estimating tibial stress throughout the duration of a treadmill run, *Med. Sci. Sports Exerc.* 51 (11) (2019 Nov) 2257–2264, <https://doi.org/10.1249/MSS.0000000000002039>. PMID: 31634292.
- [15] S.A. Meardon, J.D. Willson, S.R. Gries, T.W. Kernozek, T.R. Derrick, Bone stress in runners with tibial stress fracture, *Clin. Biomech. (Bristol, Avon)* 30 (9) (2015 Nov) 895–902, <https://doi.org/10.1016/j.clinbiomech.2015.07.012>. Epub 2015 Aug 8 PMID: 26282463.
- [16] C. Xu, A. Silder, J. Zhang, J. Hughes, G. Unnikrishnan, J. Reifman, V. Rakesh, An integrated musculoskeletal-finite-element model to evaluate effects of load carriage on the tibia during walking, *J. Biomech. Eng.* 138 (10) (2016 Oct 1), <https://doi.org/10.1115/1.4034216>. PMID: 27437640.
- [17] C. Xu, A. Silder, J. Zhang, J. Reifman, G. Unnikrishnan, A cross-sectional study of the effects of load carriage on running characteristics and tibial mechanical stress: implications for stress-fracture injuries in women, *BMC Musculoskelet. Disord.* 18 (1) (2017 Mar 23) 125, <https://doi.org/10.1186/s12891-017-1481-9>. PMID: 28330449; PMCID: PMC5363036.
- [18] C. Xu, J. Reifman, M. Baggaley, W.B. Edwards, G. Unnikrishnan, Individual differences in women during walking affect tibial response to load carriage: the importance of individualized musculoskeletal finite-element models, *IEEE Trans. Biomed. Eng.* 67 (2) (2020 Feb) 545–555, <https://doi.org/10.1109/TBME.2019.2917415>. Epub 2019 May 30 PMID: 31150325.
- [19] H. Wang, M. Kia, D.C. Dickin, Influences of load carriage and physical activity history on tibia bone strain, *J. Sport Health Sci.* 8 (5) (2019 Sep) 478–485, <https://doi.org/10.1016/j.jshs.2016.08.012>. Epub 2016 Nov 9. PMID: 31534823; PMCID: PMC6742624.
- [20] I.T. Haider, M. Baggaley, W.B. Edwards, Subject-specific finite element models of the tibia with realistic boundary conditions predict bending deformations consistent with in vivo measurement, *J. Biomech. Eng.* 142 (2) (2020 Feb 1), 021010, <https://doi.org/10.1115/1.4044034>. PMID: 31201743.
- [21] G. Unnikrishnan, C. Xu, M. Baggaley, J. Tong, S. Kulkarni, W.B. Edwards, J. Reifman, Effects of body size and load carriage on lower-extremity biomechanical responses in healthy women, *BMC Musculoskelet. Disord.* 22 (1) (2021 Feb 24) 219, <https://doi.org/10.1186/s12891-021-04076-0>. PMID: 33627093; PMCID: PMC7905550.
- [22] M.E. Kersh, S. Martelli, R. Zebaze, E. Seeman, M.G. Pandy, Mechanical loading of the femoral neck in human locomotion, *J. Bone Miner. Res.* 33 (11) (2018 Nov) 1999–2006, <https://doi.org/10.1002/jbmr.3529>. Epub 2018 Jul 18 PMID: 29920773.
- [23] P. Pellikaan, G. Giarmatzis, J. Vander Sloten, S. Verschuere, I. Jonkers, Ranking of osteogenic potential of physical exercises in postmenopausal women based on femoral neck strains, *PLoS One* 13 (4) (2018 Apr 4), e0195463, <https://doi.org/10.1371/journal.pone.0195463>. PMID: 29617448; PMCID: PMC5884624.
- [24] C. Bitsakos, J. Kerner, I. Fisher, A.A. Amis, The effect of muscle loading on the simulation of bone remodelling in the proximal femur, *J. Biomech.* 38 (1) (2005 Jan) 133–139, <https://doi.org/10.1016/j.jbiomech.2004.03.005>. PMID: 15519348.
- [25] M. Khan, K. Madden, M.T. Burrus, J.P. Rogowski, J. Stotts, M.J. Samani, R. Sikka, A. Bedi, Epidemiology and impact on performance of lower extremity stress injuries in professional basketball players, *Sports Health* 10 (2) (2018) 169–174, <https://doi.org/10.1177/1941738117738988>. Epub 2021 Feb 26. PMID: 33635519; PMCID: PMC8316280.
- [26] T.W. Dorn, A.G. Schache, M.G. Pandy, Muscular strategy shift in human running: dependence of running speed on hip and ankle muscle performance, *J. Exp. Biol.* 215 (Pt 11) (2012 Jun 1) 1944–1956, <https://doi.org/10.1242/jeb.064527>. Erratum in: *J. Exp. Biol.* 2012 Jul 1;215(Pt 13):2347. PMID: 22573774.
- [27] S.J. Warden, C.S. Wright, R.K. Fuchs, Bone microarchitecture and strength adaptation to physical activity: a within-subject controlled HRpQCT study, *Med. Sci. Sports Exerc.* 53 (6) (2021 Jun 1) 1179–1187, <https://doi.org/10.1249/MSS.0000000000002571>. PMID: 33394902.
- [28] S.J. Warden, S.M. Mantilla Roosa, M.E. Kersh, A.L. Hurd, G.S. Fleisig, M.G. Pandy, R.K. Fuchs, Physical activity when young provides lifelong benefits to cortical bone size and strength in men, *Proc. Natl. Acad. Sci. U. S. A.* 111 (14) (2014 Apr 8) 5337–5342, <https://doi.org/10.1073/pnas.1321605111>. Epub 2014 Mar 24. PMID: 24706816; PMCID: PMC3986122.
- [29] A. Seth, J.L. Hicks, T.K. Uchida, A. Habib, C.L. Dembia, J.J. Dunne, C.F. Ong, M. S. DeMers, A. Rajagopal, M. Millard, S.R. Hamner, E.M. Arnold, J.R. Yong, S. K. Lakshminathan, M.A. Sherman, J.P. Ku, S.L. Delp, OpenSim: simulating musculoskeletal dynamics and neuromuscular control to study human and animal movement, *PLoS Comput. Biol.* 14 (7) (2018 Jul 26), e1006223, <https://doi.org/10.1371/journal.pcbi.1006223>. PMID: 30048444; PMCID: PMC6061994.
- [30] S.L. Delp, F.C. Anderson, A.S. Arnold, P. Loan, A. Habib, C.T. John, E. Guendelman, D.G. Thelen, OpenSim: open-source software to create and analyze dynamic simulations of movement, *IEEE Trans. Biomed. Eng.* 54 (11) (2007 Nov) 1940–1950, <https://doi.org/10.1109/TBME.2007.901024>. PMID: 18018689.
- [31] S.L. Delp, J.P. Loan, M.G. Hoy, F.E. Zajac, E.L. Topp, J.M. Rosen, An interactive graphics-based model of the lower extremity to study orthopaedic surgical procedures, *IEEE Trans. Biomed. Eng.* 37 (8) (1990 Aug) 757–767, <https://doi.org/10.1109/10.102791>. PMID: 2210784.
- [32] E.F. Morgan, H.H. Bayraktar, T.M. Keaveny, Trabecular bone modulus-density relationships depend on anatomic site, *J. Biomech.* 36 (7) (2003 Jul) 897–904, [https://doi.org/10.1016/s0021-9290\(03\)00071-x](https://doi.org/10.1016/s0021-9290(03)00071-x). PMID: 12757797.
- [33] F. Taddei, E. Schileo, B. Helgason, L. Cristofolini, M. Viceconti, The material mapping strategy influences the accuracy of CT-based finite element models of bones: an evaluation against experimental measurements, *Med. Eng. Phys.* 29 (9) (2007 Nov) 973–979, <https://doi.org/10.1016/j.medengphy.2006.10.014>. Epub 2006 Dec 12 PMID: 17169598.
- [34] M. Ghosh, B.U. Chowdhury, M.S. Parvej, A.M. Afsar, Modeling and analysis of elastic fields in tibia and fibula, in: *AIP Conference Proceedings* 1919, AIP Publishing LLC, 2017 Dec 28, p. 020016. No. 1.
- [35] M. Mates, Atlas of anatomy: general anatomy and musculoskeletal system, *Occup. Ther. Health Care.* 22 (4) (2008) 76–77, <https://doi.org/10.1080/07380570802244514>. PMID: 23930761.
- [36] D.E. Attarian, H.J. McCrackin, D.P. DeVito, J.H. McElhaney, W.E. Garrett Jr., Biomechanical characteristics of human ankle ligaments, *Foot Ankle.* 6 (2) (1985 Oct) 54–58, <https://doi.org/10.1177/107110078500600202>. PMID: 4065775.
- [37] C. Milgrom, A. Finestone, A. Simkin, I. Ekenman, S. Mendelson, M. Millgram, M. Nyska, E. Larsson, D. Burr, In-vivo strain measurements to evaluate the strengthening potential of exercises on the tibial bone, *J. Bone Joint Surg. Br.* 82 (4) (2000 May) 591–594, <https://doi.org/10.1302/0301-620x.82b4.9677>. PMID: 10855890.
- [38] C. Milgrom, A. Simkin, A. Eldad, M. Nyska, A. Finestone, Using bone's adaptation ability to lower the incidence of stress fractures, *Am. J. Sports Med.* 28 (2) (2000 Mar-Apr) 245–251, <https://doi.org/10.1177/03635465000280021701>. PMID: 10751003.

- [39] C. Yan, S.G. Moshage, M.E. Kersh, Play during growth: the effect of sports on bone adaptation, *Curr. Osteoporos. Rep.* 18 (6) (2020 Dec) 684–695, <https://doi.org/10.1007/s11914-020-00632-0>. Epub 2020 Oct 21 PMID: 33084999.
- [40] A.F. Carbuhn, T.E. Fernandez, A.F. Bragg, J.S. Green, S.F. Crouse, Sport and training influence bone and body composition in women collegiate athletes, *J. Strength Cond. Res.* 24 (7) (2010 Jul) 1710–1717, <https://doi.org/10.1519/JSC.0b013e3181d09eb3>. PMID: 20453684.
- [41] S.J. Warden, J.A. Hurst, M.S. Sanders, C.H. Turner, D.B. Burr, J. Li, Bone adaptation to a mechanical loading program significantly increases skeletal fatigue resistance, *J. Bone Miner. Res.* 20 (5) (2005 May) 809–816, <https://doi.org/10.1359/JBMR.041222>. Epub 2004 Dec 20 PMID: 15824854.
- [42] S.A. Meardon, T.R. Derrick, Effect of step width manipulation on tibial stress during running, *J. Biomech.* 47 (11) (2014 Aug 22) 2738–2744, <https://doi.org/10.1016/j.jbiomech.2014.04.047>. Epub 2014 May 21 PMID: 24935171.
- [43] R. Kijowski, J. Choi, K. Shinki, A.M. Del Rio, A. De Smet, Validation of MRI classification system for tibial stress injuries, *AJR Am. J. Roentgenol.* 198 (4) (2012 Apr) 878–884, <https://doi.org/10.2214/AJR.11.6826>. PMID: 22451555.
- [44] A. Nattiv, G. Kennedy, M.T. Barrack, A. Abdelkerim, M.A. Goolsby, J.C. Arends, L. L. Seeger, Correlation of MRI grading of bone stress injuries with clinical risk factors and return to play: a 5-year prospective study in collegiate track and field athletes, *Am. J. Sports Med.* 41 (8) (2013 Aug) 1930–1941, <https://doi.org/10.1177/0363546513490645>. Epub 2013 Jul 3. PMID: 23825184; PMCID: PMC4367232.
- [45] C.A. Pattin, W.E. Caler, D.R. Carter, Cyclic mechanical property degradation during fatigue loading of cortical bone, *J. Biomech.* 29 (1) (1996 Jan) 69–79, [https://doi.org/10.1016/0021-9290\(94\)00156-1](https://doi.org/10.1016/0021-9290(94)00156-1). PMID: 8839019.
- [46] M. Fredericson, J. Ngo, K. Cobb, Effects of ball sports on future risk of stress fracture in runners, *Clin. J. Sport Med.* 15 (3) (2005 May) 136–141, <https://doi.org/10.1097/01.jsm.0000165489.68997.60>. PMID: 15867555.
- [47] W.B. Edwards, T.J. Schnitzer, K.L. Troy, Torsional stiffness and strength of the proximal tibia are better predicted by finite element models than DXA or QCT, *J. Biomech.* 46 (10) (2013 Jun 21) 1655–1662, <https://doi.org/10.1016/j.jbiomech.2013.04.016>. Epub 2013 May 13. PMID: 23680350; PMCID: PMC3676700.